International Journal of Nanomedicine

Dovepress
open access to scientific and medical research

Open Access Full Text Article

ORIGINAL RESEARCH

The characteristic $Ag_{core}Au_{shell}$ nanoparticles as SERS substrates in detecting dopamine molecules at various pH ranges

This article was published in the following Dove Press journal:
International Journal of Nanomedicine
25 August 2015
Number of times this article has been viewed

Yanru Bu[1]
Sang-Wha Lee[2]

[1]Department of Chemical Engineering, Faculty of Engineering, Monash University, Melbourne, VIC, Australia; [2]Department of Chemical and Biochemical Engineering, Gachon University, Seongnam-si, Gyeonggi-do, Republic of Korea

Abstract: $Ag_{core}Au_{shell}$ nanoparticles (NPs) are a promising surface-enhanced Raman scattering (SERS) substrate, which can offer a high enhancement factor through the combined effect of the high SERS activity of the Ag core and the biocompatibility of the Au shell. In this study, $Ag_{core}Au_{shell}$ NPs were examined as SERS substrates for the sensitive detection of dopamine (DA) molecules in an aqueous solution. The SERS activity of the $Ag_{core}Au_{shell}$ NPs was strongly dependent on the pH of the solution. When the pH of the solution was acidic (pH <5) or basic (pH >9), the $Ag_{core}Au_{shell}$ NPs exhibited negligible SERS activity toward the DA molecules, due to the weakened interactions (or repulsive forces) between the DA molecules and the core–shell NPs. On the other hand, the $Ag_{core}Au_{shell}$ NPs exhibited a high SERS activity in the intermediate pH ranges (pH 7–9), due to the molecular bridging effect of DA molecules, which allows probe molecules to be located at the interstitial junctions (so-called hot spots) between the core–shell NPs. The results of this study highlight the importance of probe-induced clustering of core–shell NPs in the SERS measurements at physiological pH.

Keywords: dopamine, $Ag_{core}Au_{shell}$ NPs, solution pH, SERS activity

Introduction

Noble metals (Au and Ag) nanoparticles (NPs) are widely used as optical sensing agents for bio-recognition because of their intense visible-region absorption, which is mainly attributed to surface plasmon resonance (SPR).[1–3] The core–shell NPs often exhibit enhanced physico-chemical properties (such as optical, electronic, and catalytic properties) over their monometallic counterparts, as a result of the localized electric field enhancement in the core–shell nanostructure.[4–6] The plasmonic core–shell NPs can also have a strong absorption in the near-infrared region, which can lead to a photothermal effect, consequently interplaying as a theranostic particle system with diagnostic and therapeutic capability.[7–9] Surface-enhanced Raman scattering (SERS) is a promising and highly sensitive and selective optical analysis technique.[10,11] It can markedly enhance the Raman signals of probe molecules by a factor of 10^6–10^{14}, thus enabling the detection even of a single molecule.[12–15]

$Ag_{core}Au_{shell}$ plasmonic NPs are a promising SERS substrate, which can offer a high enhancement factor through the synergy of the Ag core and the Au shell.[16,17] In particular, the Ag core displays a high SERS activity because of the long-range effect via significant electromagnetic enhancement, and the Au shell exhibits biocompatible stability in an aqueous solution. Thus, $Ag_{core}Au_{shell}$ NPs could offer a high enhancement factor in SERS measurements through the combined effect of the high SERS activity of the Ag core and the biocompatibility of the Au shell.[4,18–20] There are many

Correspondence: Sang-Wha Lee
Department of Chemical and Biochemical Engineering, Gachon University, Seongnam-daero 1342, Sujeong-gu, Seongnam si, Gyeonggi-do, Republic of Korea 461-701
Tel +82 31 750 5360
Fax +82 31 750 5363
Email lswha@gachon.ac.kr

factors (including solution pH, inter-particle spacing, particle size, and localized SPR), which can also influence the SERS activity of the core–shell NPs.[16,21–25] The systematic investigation of the correlation between the aforementioned factors and the SERS activity of core–shell NPs is of great significance for the realization of highly efficient and reliable SERS substrates.

Dopamine (DA) is a monoamine neurotransmitter in the catecholamine family, which plays a number of important physiological roles in animals. In the brain, DA functions as a neurotransmitter – a chemical released by nerve cells to send signals to other nerve cells. Several serious diseases of the nervous system are associated with dysfunctions of the DA system, such as Parkinson's disease, schizophrenia, and attention deficit hyperactivity disorder.[26–28] For the early diagnosis of these conditions, it is very important to determine the DA concentration levels (0.01−1.0 μM) from the extracellular fluid. In this regard, SERS measurements using metal colloids are advantageous owing to easy preparation, fast detection, and homogeneous reactions.[22,29]

This work mainly focus on the influence of particle size and solution pH on the sensitive detection of DA molecules using $Ag_{core}Au_{shell}$ NPs as SERS substrates. The maximal SERS activity of the core–shell NPs was obtained at an appropriate particle size and pH range (pH 7–9), highlighting the importance of probe-induced clustering of colloidal NPs for their enhanced SERS activity at physiological pH ranges. Prepared samples were analyzed by dynamic light scattering, scanning electron microscopy (SEM), ultraviolet-visible (UV-vis) spectrometry, and micro-Raman spectroscopy (laser excitation at 632.8 nm) in order to characterize their size, morphology, and optical properties.

Materials and methods

Chemical materials

All the chemicals used were purchased from Aldrich Company, Wyoming, IL, USA: chloroauric acid ($HAuCl_4$), silver nitrate ($AgNO_3$), sodium citrate ($Na_3C_6H_5O_7$), hydroxylamine hydrochloride ($NH_2OH{\cdot}HCl$), high-performance liquid chromatography grade water (H_2O), and DA hydrochloride ($C_8H_{11}NO_2{\cdot}HCl$). All the reagents were analytically pure.

Synthesis of Ag NPs

Ag NPs were prepared according to the citrate reduction method.[25] The particle size was controlled by adjusting the concentration of citrate ions relative to the concentration of ionized silver complex in an aqueous solution. The Ag NPs (20–50 nm) were obtained by injecting aliquots (2–5 mL) of 1.0% sodium citrate (w/v) into 100 mL of boiling water containing 1.0% $AgNO_3$ (w/v in 1.0 mL) with vigorous stirring. The mixture was kept boiling for an additional 10 minutes and then transferred to a cold plate. The stirring was maintained until the solution cooled down to room temperature.

Synthesis of $Ag_{core}Au_{shell}$ NPs

A two-step reduction in an aqueous solution was used for the preparation of the gold-coated silver NPs. In brief, 12.5 mL of Ag precursor was diluted with 10 mL of high-performance liquid chromatography grade water, and then x mL of $NH_2OH{\cdot}HCl$ (6.25×10^{-3} M) and x mL of $HAuCl_4$ (4.65×10^{-4} M) were added drop-wise into the aqueous solution at an approximate rate of 2 mL/min, using two separate pipettes with vigorous stirring. The stirring continued for 45 minutes. In this work, $Ag_{core}Au_{shell}$ NPs were prepared by injecting 6 mL of $NH_2OH{\cdot}HCl$ (6.25×10^{-3} M) and 5 mL of $HAuCl_4$ (4.65×10^{-4} M) into the solution containing preformed Ag NPs, respectively.

Instrumental analysis

UV-vis spectroscopy (HP 8453, Agilent Technologies, Santa Clara, CA, USA) was used to characterize the absorption spectra of the sample in the wavelength ranges of 200–1,000 nm. The particle size was measured at ambient temperature using the intensity-based dynamic light scattering method. Field emission-SEM (Hitachi Ltd., Tokyo, Japan) was also employed to investigate the size and morphology of prepared samples. Transmission electron microscopy (TEM, AP Tech, McMinnville, OR, USA, Tecnai, G2 F30 S-Twin) was performed to confirm the existence of the core–shell nanostructure of prepared samples using an accelerating voltage of 300 kV. A Monora500i micro Raman spectrometer (ANDOR, Belfast, UK) was used to characterize the optical properties of these NPs. The Raman spectrograph employed a 1,200 g/mm grating and laser excitation at 632.8 nm with accumulation times of 5 seconds.

Results and discussion

The $Ag_{core}Au_{shell}$ NPs with tunable plasmon resonances were prepared via an electron-less plating of Au layered over Ag colloids of different sizes (25, 38, and 53 nm). The freshly prepared solution indicate the pH 5 and zeta potential of –15.43±7.32 mV. Figure 1 demonstrates the surface plasmon-derived absorption peaks (or plasmon peaks) located at 516, 559, and 593 nm, corresponding to the core sizes of 25, 38, and 53 nm, respectively. The plasmon peak of core–shell NPs is significantly red-shifted from a typical

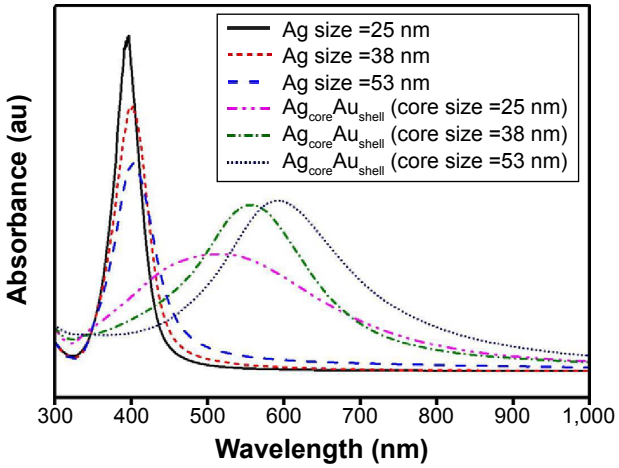

Figure 1 The UV-vis spectra of the $Ag_{core}Au_{shell}$ NPs with Ag NPs with different core sizes (25, 38, and 53 nm) at pH 5. The UV-vis spectra of singular Ag NPs (38 nm) is included for comparison, in which the maximum peak position is located at approximately 400 nm.
Abbreviations: au, arbitrary unit; NPs, nanoparticles; UV-vis, ultraviolet-visible.

absorption peak of Ag NPs (approximately 400 nm), and the red-shift of plasmon bands increases with the increment of the core size. Notably, all the plasmon bands display one broad spectrum, indicative of the successful synthesis of the core–shell nanostructures.

Figure 2 shows the SEM and TEM images of the Ag NPs and the $Ag_{core}Au_{shell}$ NPs with Ag NPs of various core sizes. Figure 2A and D demonstrates the SEM image of the 25 nm Ag NPs and the corresponding TEM image of the $Ag_{core}Au_{shell}$ NPs. Figure 2B and E displays the SEM image of the 38 nm Ag NPs and the corresponding TEM image of the $Ag_{core}Au_{shell}$ NPs. Figure 2C and F demonstrates the SEM image of the 53 nm Ag NPs and the corresponding TEM image of the $Ag_{core}Au_{shell}$ NPs. The Au shell was formed by adding 5 mL of $HAuCl_4$ (4.65×10^{-4} M) and 6 mL of $NH_2OH{\cdot}HCl$ (6.25×10^{-3} M). When preparing the Ag NPs and the $Ag_{core}Au_{shell}$ NPs, the reducing agents are excessive so that the Au and Ag precursors are completely reduced. According to the TEM images showing a clear core–shell contrast, the core–shell ratio of the $Ag_{core}Au_{shell}$ NPs (Ag core =53 nm) is smaller than those of the $Ag_{core}Au_{shell}$ NPs (Ag core =25 or 38 nm) with a similar core–shell ratio, as shown in Figure 2D–F. In addition, there are no pinholes on the surface of the core–shell NPs, probably due to the full coverage of the Au layer over the Ag core. In the following section, the core size of Ag NPs will be described by the number in parentheses, without expressing "Ag core size".

Figure 3 demonstrates the SERS signals of the DA molecules adsorbed onto the $Ag_{core}Au_{shell}$ NPs with different core sizes (25, 38, and 53 nm) at pH 7. The band at ~1,480 cm^{-1} is assigned to the ring stretching vibration attributed to the stretching of the OC–CO bonds, and the band at 1,320 cm^{-1} is assigned to ring stretching vibration.[30,31] In particular, the ring stretching vibration/deformation mode of the OH bonds is clearly apparent at 1,370 cm^{-1}.[32] It is generally known that the SERS signal is maximized when the excitation is conducted at a wavelength close to the plasmon resonance frequency.[33]

As shown in Figure 3, the $Ag_{core}Au_{shell}$ NPs (25 nm) with a plasmon peak at 516 nm exhibit much lower SERS activity than the $Ag_{core}Au_{shell}$ NPs (38 or 53 nm) with more red-shifted

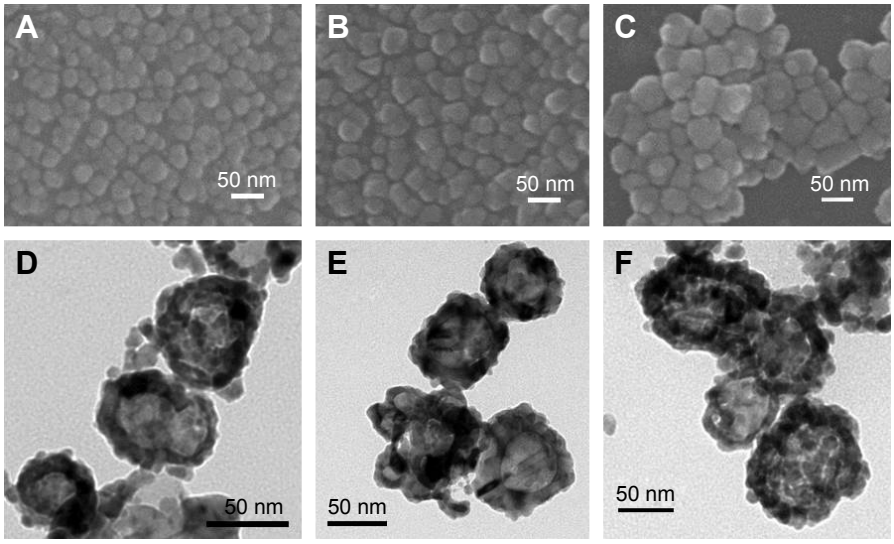

Figure 2 SEM and TEM images of the Ag NPs and the $Ag_{core}Au_{shell}$ NPs prepared with various Ag core sizes.
Notes: (**A** and **D**) SEM images of the 25 nm Ag NPs and related TEM images of the $Ag_{core}Au_{shell}$ NPs, respectively. (**B** and **E**) SEM images of the 38 nm Ag NPs and related TEM images of the $Ag_{core}Au_{shell}$ NPs, respectively. (**C** and **F**) SEM images of the 53 nm Ag NPs and related TEM images of the $Ag_{core}Au_{shell}$ NPs, respectively. The Au shell was formed by adding 5 mL of $HAuCl_4$ (4.65×10^{-4} M) and 6 mL of $NH_2OH{\cdot}HCl$ (6.25×10^{-3} M).
Abbreviations: SEM, scanning electron microscopy; TEM, transmission electron microscopy; NPs, nanoparticles.

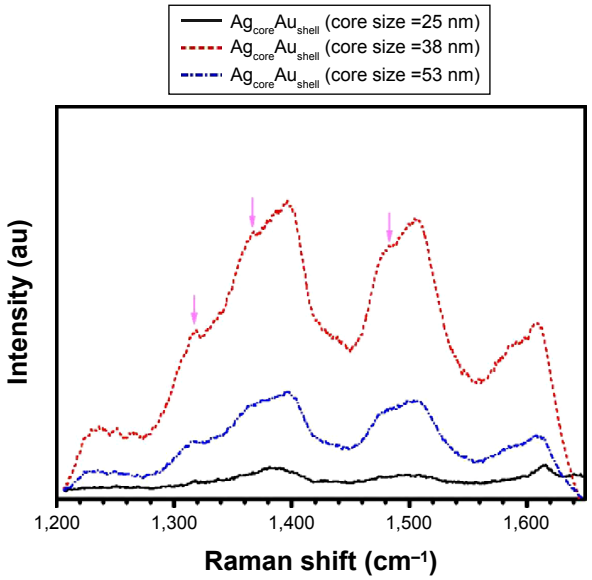

Figure 3 Raman spectra of DA (1×10^{-4} M) adsorbed on Ag$_{core}$Au$_{shell}$ NPs with core Ag NPs of different sizes (25, 38, and 53 nm) at pH 7.
Notes: The arrows indicate the characteristic Raman signals of DA molecules at 1,320, 1,370, and 1,480 cm^{-1}.
Abbreviations: au, arbitrary unit; DA, dopamine; NPs, nanoparticles.

plasmon bands at 559 and 593 nm, which are indicative of the importance of the plasmon resonance-assisted SERS effects.[19,22,34] Conversely, the Ag$_{core}$Au$_{shell}$ NPs (38 nm) exhibit higher SERS activity than Ag$_{core}$Au$_{shell}$ NPs (53 nm) with a plasmon band that is closer to the excitation wavelength of 633 nm. The SERS activity of the core–shell NPs is also dependent on the particle size, showing the key role of the particle size in the SERS measurements under plasmon resonance-assisted conditions.[16,18,35–37]

Figure 4A and B demonstrates the pH-dependent changes in the UV-vis spectra of the Ag$_{core}$Au$_{shell}$ NPs (38 nm) in the absence or presence of DA molecules. As the solution pH increases without DA molecules, the plasmon band of the Ag$_{core}$Au$_{shell}$ NPs is gradually blue-shifted. This shift indicates the collapse of the partial aggregation into monodispersed core–shell NPs, which is attributed to repulsive interactions between the core–shell NPs (Figure 4A). In the presence of DA molecules (10^{-4} M), the Ag$_{core}$Au$_{shell}$ NPs also exhibit a blue-shift in the primary absorption bands when the pH changed

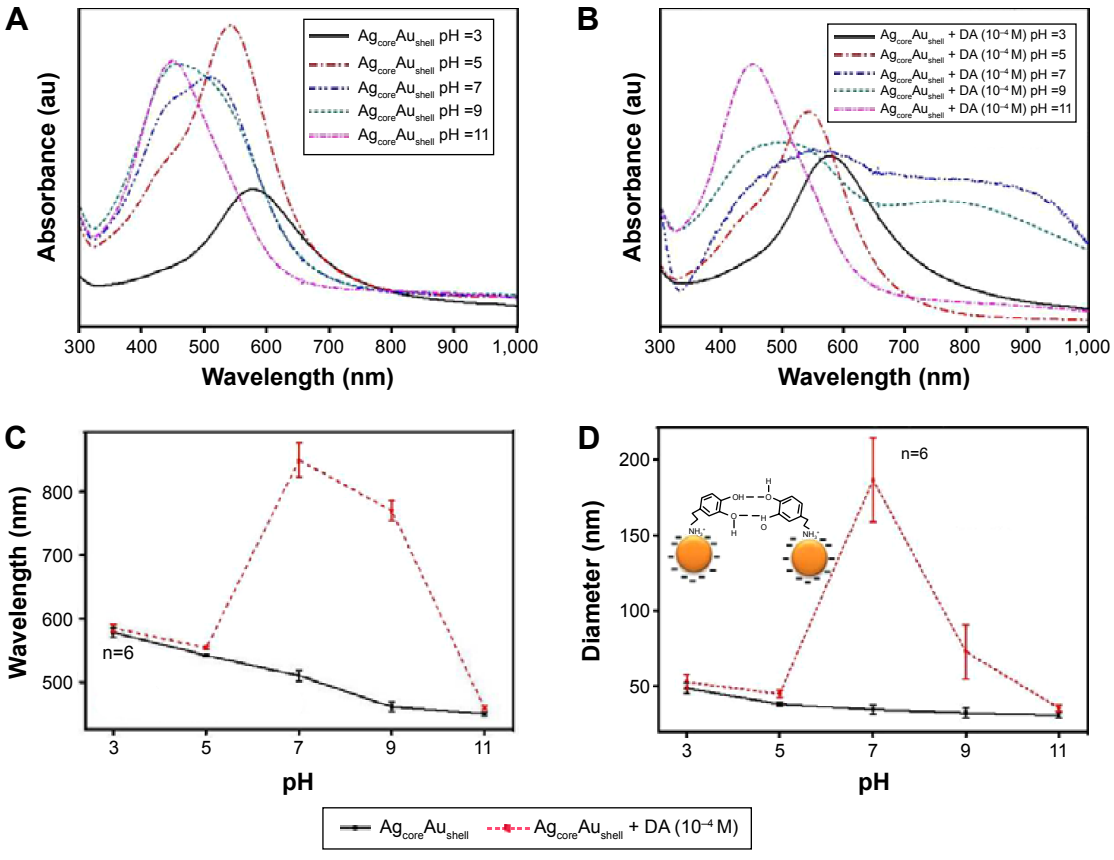

Figure 4 Physico-chemical properties of core-shell Ag$_{core}$Au$_{shell}$ NPs.
Notes: (**A**) The UV-vis spectra of Ag$_{core}$Au$_{shell}$ NPs (38 nm) at various pH ranges. (**B**) The UV-vis spectra of Ag$_{core}$Au$_{shell}$ NPs with DA (10^{-4} M) at various pH ranges. (**C**) The absorption maximum of Ag$_{core}$Au$_{shell}$ NPs with and without DA (10^{-4} M) at various pH ranges. (**D**) The particle size of Ag$_{core}$Au$_{shell}$ NPs with and without DA (10^{-4} M) at various pH ranges.
Abbreviations: au, arbitrary unit; DA, dopamine; NPs, nanoparticles; UV-vis, ultraviolet-visible.

from pH 3 to pH 5, as shown in Figure 4B. At the intermediate pH ranges (pH 7–9), however, the presence of DA molecules induces the aggregation of core–shell NPs and thereby generates a secondary peak at a longer wavelength (>650 nm) attributed to the plasmon coupling of aggregated particles.[38,39] A further increase in the solution pH again induces a blue-shift of the primary absorption band with the simultaneous disappearance of the secondary peak at the longer wavelength, due to the repulsive dispersion of core–shell NPs.

Figure 4C shows the difference in the peak position of primary absorption bands obtained from colloidal solutions at various pH levels before and after DA addition. At the intermediate pH ranges (pH 7–9), the absorption peak is red-shifted by approximately 30−40 nm. This shift indicates the partial aggregation of particles by the cross-linking effect of DA molecules.[40,41] In other words, one terminal amine group attaches to the individual core–shell NPs and the remaining hydroxyl groups interact with each other via a hydrogen bonding network, consequently leading to the aggregation of core–shell NPs.[4] In contrast, there is no distinct change in the peak position when the solution pH deviates from the intermediate pH range, indicating the negligible cross-linking effects by the DA molecules.

Figure 4D demonstrates the change of the particle size as a function of solution pH. In the absence of DA, the particle size slightly decreases by 21% as the pH increases from pH 3 to pH 11. This change is to be expected from the increased repulsive dispersion due to the increase in negative surface charge states. In the presence of DA, however, the particle size significantly increases to 187 nm from 73 nm at pH 7 and pH 9, respectively. This increase is because the Au shell is negatively charged and the DA is positively charged at the intermediate pH ranges. In other words, the positively charged DA plays a role as a cross-linker via hydrogen-mediated interactions between the hydroxyl groups of DA molecules that are electrostatically attached to the $Ag_{core}Au_{shell}$ NPs via amine groups, according to the inset shown in Figure 4D. In practice, DA is N-protonated (H_3DA^+) (pH <9.05), but negatively charged under basic pH conditions.[4]

The zeta potential of the freshly prepared $Ag_{core}Au_{shell}$ NPs is −15.43±7.32 mV at pH 5. When the pH of the solution changes to pH 10, the zeta potential increases to −45.68±7.32 mV. This shift implies that the surface charge of the $Ag_{core}Au_{shell}$ NPs strongly depends on the pH of the solution. The increase in the solution pH induces more negative charges on the $Ag_{core}Au_{shell}$ NPs, leading to more repulsive forces between the core–shell NPs, and thereby maintaining their monodispersed states. The slight increase in the particle size under acidic pH conditions is attributed to the neutralization effect by the hydrogen ions attached to the negatively charged particles, resulting in the slight aggregation of the core–shell particles, as shown in Figure 4D.

Figure 5 shows the Raman spectra of the DA (1×10^{-4} M) adsorbed on the $Ag_{core}Au_{shell}$ NPs as a function of the solution pH. The SERS activity of the $Ag_{core}Au_{shell}$ NPs is maximized at pH 9. At higher pH (pH >9), an abrupt decrease in the SERS activity occurs because of the repulsive interactions between the DA molecules and the $Ag_{core}Au_{shell}$ NPs. Low pH levels (pH 3–5) also decrease the SERS intensity because of the negligible adsorption of DA molecules on the $Ag_{core}Au_{shell}$ NPs. At intermediate pH ranges (pH 7–9), some degree of particle aggregation occurs due to the cross-linking effect of DA molecules, generating effective hot spots at the interstitial junctions between the core–shell NPs.[16] Meanwhile, the SERS activity decreases at pH 7 because of the heavy aggregation of the core–shell NPs, which may reduce the effectiveness of hot spots in detecting DA molecules.

Figure 6 illustrates the pH-dependent interaction of the $Ag_{core}Au_{shell}$ NPs with DA molecules at various pH ranges: i) at low pH levels (pH <5), the $Ag_{core}Au_{shell}$ NPs are less negatively charged because of the neutralization effect by the hydrogen ions, ie, the zeta potential of the NPs is −8.58±8.42 mV at pH 3. Thus, the cross-linking effect of adsorbed DA is fairly weakened, resulting in a slight aggregation of core–shell NPs. ii) At an intermediate pH range (pH 7–9), the $Ag_{core}Au_{shell}$ NPs are more negatively charged and the DA is positively charged, inducing electrostatic interactions between the $Ag_{core}Au_{shell}$ NPs and the DA molecules. Thus,

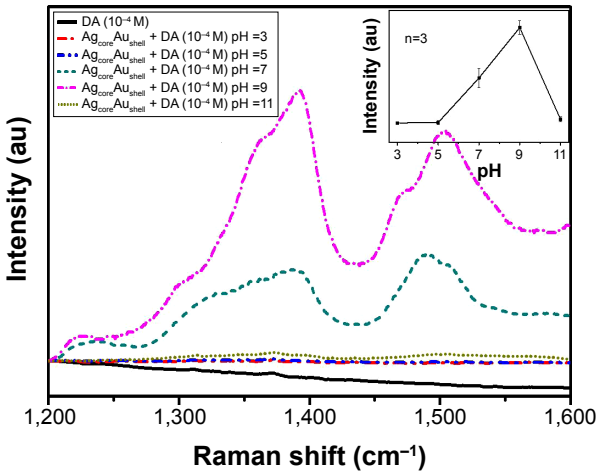

Figure 5 Raman spectra of DA (1×10^{-4} M) adsorbed on $Ag_{core}Au_{shell}$ NPs at various pH levels.

Notes: The inset presents the Raman intensity of the $Ag_{core}Au_{shell}$ NPs with DA as a function of solution pH.

Abbreviations: au, arbitrary unit; DA, dopamine; NPs, nanoparticles.

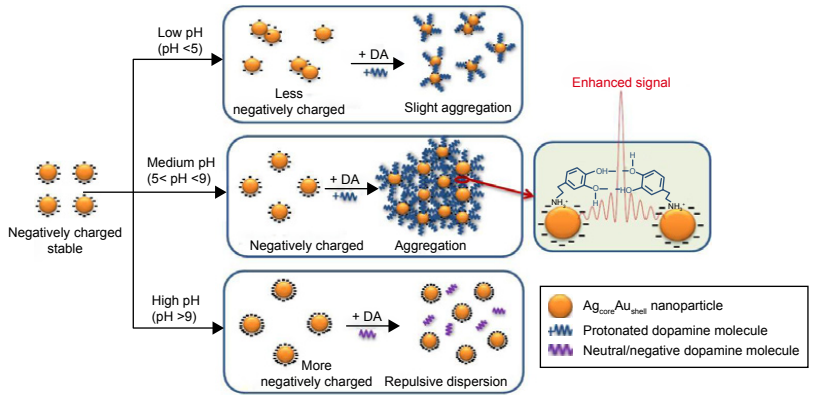

Figure 6 The aggregation behavior of $Ag_{core}Au_{shell}$ NPs with and without DA molecules at various pH ranges.
Abbreviations: DA, dopamine; NPs, nanoparticles.

DA molecules are effectively adsorbed on the $Ag_{core}Au_{shell}$ NPs as cross-linkers which can enhance the SERS signals by providing effective hot spots at the interstitial junctions between the core–shell NPs. iii) At high pH levels (pH >9), the DA presents in neutral or negatively charged states, ie, the zeta potential of the NPs is –45.68±14.75 mV at pH 10. Thus, DA adsorption is significantly reduced owing to the repulsive interactions against the negatively charged core–shell NPs.

In summary, $Ag_{core}Au_{shell}$ NPs are a promising SERS substrate, which can offer a high enhancement factor through the combined effect of high SERS activity of the Ag core and biocompatibility of the Au shell. This work mainly investigated the effect of Ag NP core size and solution pH on the sensitive detection of DA probes at a fixed concentration (10^{-4} M). The optimal SERS activity was obtained from colloidal core–shell NPs with appropriate particle sizes at intermediate pH ranges (pH 7–9). According to Figure S1, the core–shell NPs demonstrate the detection limit of DA even down to 0.1 μM, indicative of the potential candidate of these NPs for real-life application to DA sensing. We believe that these results can provide some insight into the SERS measurement using colloidal systems, highlighting the importance of probe-induced aggregation and optimal particle size for enhanced optical properties.

Conclusion

The characteristic SERS activity of $Ag_{core}Au_{shell}$ NPs with Ag NPs of different core sizes was investigated for the sensitive detection of DA molecules at various pH levels. The $Ag_{core}Au_{shell}$ NPs (38 nm) exhibited higher SERS activity than those of $Ag_{core}Au_{shell}$ NPs (25 or 53 nm), indicating the influence of particle size on the SERS measurements. More importantly, the SERS activity of the core–shell NPs was strongly dependent on the pH of the solution. The $Ag_{core}Au_{shell}$ NPs exhibited a maximal SERS activity at intermediate ranges of pH 7–9 because the molecular bridging effect of DA molecules provided many hot spots at the interstitial junctions between the core–shell NPs. Outside the intermediate pH ranges (pH <5 or pH >9), the SERS activity decreased significantly because of the lack of DA adsorption on the core–shell NPs. Conclusively, $Ag_{core}Au_{shell}$ NPs with appropriate particle size offered many hot spots for the sensitive detection of DA molecules at intermediate pH ranges (pH 7–9), highlighting the importance of probe-induced clustering and optimal particle size for enhanced SERS activity in a colloidal system.

Acknowledgments

This work was supported by the National Research Foundation of Korea (NRF) grant funded by the Korea government (MEST) (20090093908) and by the National Research Foundation of Korea Grant funded by the Korean Government (MEST) (NRF-2010-C1AAA001-2010-0028958).

Disclosure

The authors report no conflicts of interest in this work.

References

1. Kelly KL, Coronado E, Zhao LL, Schatz GC. The optical properties of metal nanoparticles: the influence of size, shape, and dielectric environment. *J Phys Chem B*. 2003;107:668–677.
2. Daniel MC, Astruc D. Gold nanoparticles: assembly, supramolecular chemistry, quantum-size-related properties, and applications toward biology, catalysis, and nanotechnology. *Chem Rev*. 2004;104(1):293–346.
3. Huang X, Jain PK, El-Sayed IH, El-Sayed MA. Gold nanoparticles: interesting optical properties and recent applications in cancer diagnostics and therapy. *Nanomedicine*. 2007;2(5):681–693.
4. Bu Y, Lee S. Influence of dopamine concentration and surface coverage of Au shell on the optical properties of Au, Ag, and Ag(core)Au(shell) nanoparticles. *ACS Appl Mater Interfaces*. 2012;4(8):3923–3931.

5. Rivas L, Sanchez-Cortes S, García-Ramos JV, Morcillo G. Mixed silver/gold colloids: a study of their formation, morphology, and surface-enhanced Raman activity. *Langmuir*. 2000;16:9722–9728.
6. Zaera F. Outstanding mechanistic questions in heterogeneous catalysis. *J Phys Chem B*. 2002;106:4043–4052.
7. Lee J, Yang J, Ko H, et al. Multifunctional magnetic gold nanocomposites: human epithelial cancer detection via magnetic resonance imaging and localized synchronous therapy. *Adv Funct Mater*. 2008; 18(2):258–264.
8. Xia Y, Li W, Cobley CM, et al. Gold nanocages: from synthesis to theranostic applications. *Acc Chem Res*. 2011;44(10):914–924.
9. Choi J, Yang J, Jang E, et al. Gold nanostructures as photothermal therapy agent for cancer. *Anticancer Agents Med Chem* (Formerly Current Medicinal Chemistry-Anti-Cancer Agents). 2011;11(10):953–964.
10. Kneipp K, Wang Y, Kneipp H, et al. Single molecule detection using Surface-Enhanced Raman Scattering (SERS). *Phys Rev Lett*. 1997;78(9): 1667–1670.
11. Le Ru EC, Etchegoin PG. Single-molecule surface-enhanced Raman spectroscopy. *Ann Rev Phys Chem*. 2012;63:65–87.
12. Esenturk EN, Walker ARH. Surface-enhanced Raman scattering spectroscopy via gold nanostars. *J Raman Spectrosc*. 2009;40:86–91.
13. Kumar GVP, Shruthi S, Vibha B, Reddy BAA, Kundu TK, Narayana C. Hot spots in Ag core−Au shell nanoparticles potent for surface-enhanced Raman scattering studies of biomolecules. *J Phys Chem C*. 2007;111(11): 4388–4392.
14. Alvarez-Puebla RA, Liz-Marzan LM. Traps and cages for universal SERS detection. *Chem Soc Rev*. 2012;41(1):43–51.
15. Chae W-S, Yu H, Ham S-K, Lee M-J, Jung J-S, Robinson DB. Bimodal porous gold opals for molecular sensing. *Electron Mater Lett*. 2013;9(6):783–786.
16. Mandal M, Ranjan Jana N, Kundu S, Kumar Ghosh S, Panigrahi M, Pal T. Synthesis of Aucore–Agshell type bimetallic nanoparticles for single molecule detection in solution by SERS method. *J Nanopart Res*. 2004;6(1): 53–61.
17. Ma Y, Zhou J, Shu L, Li T, Petti L, Mormile P. Optimizing Au/Ag core–shell nanorods: purification, stability, and surface modification. *J Nanopart Res*. 2014;16(6).
18. Jana NR. Silver coated gold nanoparticles as new surface enhanced Raman substrate at low analyte concentration. *Analyst*. 2003;128(7):954.
19. Alvarez-Puebla RA, Ross DJ, Nazri GA, Aroca RF. Surface-enhanced Raman scattering on nanoshells with tunable surface plasmon resonance. *Langmuir*. 2005;21(23):10504–10508.
20. Cui Y, Ren B, Yao JL, Gu RA, Tian ZQ. Synthesis of AgcoreAushell bimetallic nanoparticles for immunoassay based on surface-enhanced Raman spectroscopy. *J Phys Chem B*. 2006;110(9):4002–4006.
21. McFarland AD, Young MA, Dieringer JA, Van Duyne RP. Wavelength-scanned surface-enhanced Raman excitation spectroscopy. *J Phys Chem B*. 2005;109(22):11279–11285.
22. Hossain MK, Kitahama Y, Huang GG, Han X, Ozaki Y. Surface-enhanced Raman scattering: realization of localized surface plasmon resonance using unique substrates and methods. *Anal Bioanal Chem*. 2009;394(7): 1747–1760.
23. Lee SH, Bantz KC, Lindquist NC, Oh SH, Haynes CL. Self-assembled plasmonic nanohole arrays. *Langmuir*. 2009;25(23):13685–13693.
24. Bu Y, Lee S. The optical properties of gold nanoparticles with dopamine at different hydrogen ion concentration. *J Nanosci Nanotechnol*. 2013;13(6):4178–4182.
25. Bu Y, Lee S-W. Optical properties of dopamine molecules with silver nanoparticles as surface-enhanced Raman scattering (SERS) substrates at different pH conditions. *J Nanosci Nanotechnol*. 2013;13:5992–5996.
26. Davis KL, Kahn RS, Ko G, Davidson M. Dopamine in schizophrenia: a review and reconceptualization. *Am J Psychiatry*. 1991;148:1474–1486.
27. Reisine TD, Fields JZ, Yamamura HI, et al. Neurotransmitter receptor alterations in Parkinson's disease. *Life Sciences*. 1977;21(3):335–343.
28. Shapiro MG, Westmeyer GG, Romero PA, et al. Directed evolution of a magnetic resonance imaging contrast agent for noninvasive imaging of dopamine. *Nature Biotechnol*. 2010;28(3):264–270.
29. Sarkar A, Wang H, Daniels-Race T. Surface enhanced Raman spectroscopy on silver-nanoparticle-coated carbon-nanotube networks fabricated by electrophoretic deposition. *Electronic Mater Lett*. 2014; 10(2):325–335.
30. Lee NS, Hsieh YZ, Paisley RF, Morris MD. Surface-enhanced Raman spectroscopy of the catecholamine neurotransmitters and related compounds. *Anal Chem*. 1988;60(5):442–446.
31. Volkan M, Stokes DL, Vo-Dinh T. Surface-enhanced Raman of dopamine and neurotransmitters using sol-gel substrates and polymer-coated fiber-optic probes. *Appl Spectrosc*. 2000;54(12):1842–1848.
32. Youn MY, Kim Y, Lee N. Raman spectroscopic study of monodentate dopamine adsorbed on silver and copper adatoms. *Bull Korean Chem Soc*. 1997;18:1314–1316.
33. Liu G, Li Y, Duan G, et al. Tunable surface plasmon resonance and strong SERS performances of Au opening-nanoshell ordered arrays. *ACS Appl Mater Interfaces*. 2012;4(1):1–5.
34. Zhu Z, Zhu T, Liu Z. Raman scattering enhancement contributed from individual gold nanoparticles and interparticle coupling. *Nanotechnology*. 2004;15(3):357–364.
35. Freeman RG, Hommer MB, Grabar KC, Jackson MA, Natan MJ. Ag-clad Au nanoparticles: novel aggregation, optical, and surface-enhanced Raman scattering properties. *J Phys Chem*. 1996;100(2):718–724.
36. Wei S, Wang Q, Zhu J, Sun L, Lin H, Guo Z. Multifunctional composite core-shell nanoparticles. *Nanoscale*. 2011;3(11):4474–4502.
37. Mikac L, Ivanda M, Gotić M, Mihelj T, Horvat L. Synthesis and characterization of silver colloidal nanoparticles with different coatings for SERS application. *J Nanopart Res*. 2014;16(12).
38. Storhoff JJ, Lazarides AA, Mucic RC, Mirkin CA, Letsinger RL, Schatz GC. What controls the optical properties of DNA-linked gold nanoparticle assemblies? *J Am Chem Soc*. 2000;122(19):4640–4650.
39. Kreibig U, Genzel L. Optical absorption of small metallic particles. *Surface Science*. 1985;156:678–700.
40. Mandal S, Gole A, Lala N, Gonnade R, Ganvir V, Sastry M. Studies on the reversible aggregation of cysteine-capped colloidal silver particles interconnected via hydrogen bonds. *Langmuir*. 2001;17(20): 6262–6268.
41. Zhang Y, Li B, Chen X. Simple and sensitive detection of dopamine in the presence of high concentration of ascorbic acid using gold nanoparticles as colorimetric probes. *Microchim Acta*. 2009;168(1–2):107–113.

Supplementary material

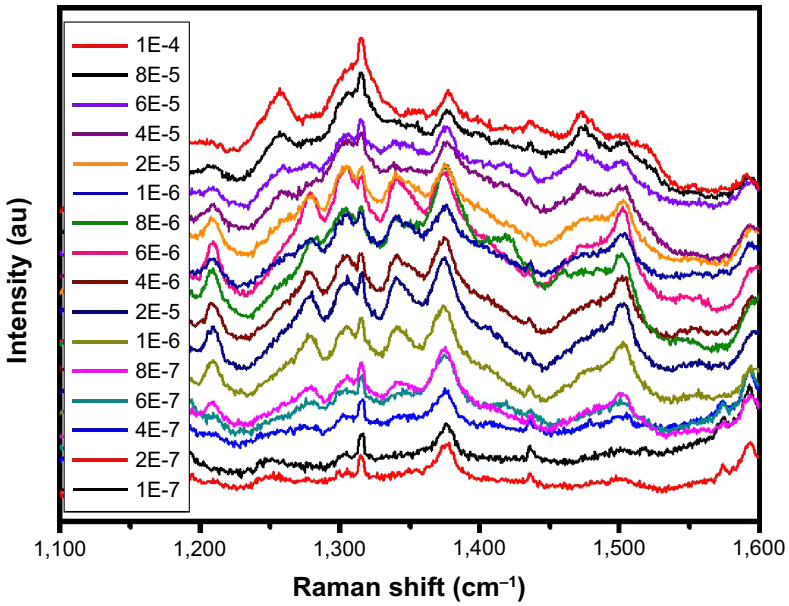

Figure S1 Raman spectra of different concentrations of DA (1×10^{-7} to 1×10^{-3} M) adsorbed on $Ag_{core}Au_{shell}$ NPs with the core size of 38 nm.
Abbreviations: DA, dopamine; NPs, nanoparticles.